

Oxygen ordering in the high- T_c superconductor $\text{HgBa}_2\text{CaCu}_2\text{O}_{6+\delta}$ as revealed by perturbed angular correlation

T. M. Mendonça,^{1,2,*} J. G. Correia,^{3,4} H. Haas,³ P. Odier,² P. B. Tavares,⁵ M. R. da Silva,⁴ A. M. L. Lopes,⁴ A. M. Pereira,¹ J. N. Gonçalves,⁶ J. S. Amaral,⁶ C. Darie,² and J. P. Araujo¹

¹*IFIMUP and IN—Institute of Nanosciences and Nanotechnologies, Rua do Campo Alegre 687, P-4169-007 Porto, Portugal*

²*Institut Néel, CNRS, Avenue des Martyrs 25, F-38042 Grenoble Cedex 9, France*

³*Instituto Tecnológico e Nuclear, E.N. 10—Apartado 21, P-2686-953 Sacavém, Portugal*

⁴*Centro de Física Nuclear da Universidade de Lisboa, Avenida Prof. Gama Pinto 2, P-1649-002 Lisboa, Portugal*

⁵*Centro de Química-Vila Real, Departamento de Química, Universidade de Trás-os-Montes e Alto Douro, P-5001-911 Vila Real, Portugal*

⁶*Departamento de Física and CICECO, Universidade de Aveiro, Campus Universitário de Santiago, P-3810-193 Aveiro, Portugal*

(Received 2 August 2010; revised manuscript received 23 June 2011; published 23 September 2011)

Lattice sites and collective ordering of oxygen atoms in $\text{HgBa}_2\text{CaCu}_2\text{O}_{6+\delta}$ were studied using the perturbed angular correlation (PAC) technique at ISOLDE/CERN. The electric field gradients (EFG) at $^{199\text{m}}\text{Hg}$ nuclei have been measured as functions of oxygen doping on the Hg planes, above and below T_c . In comparison with the results obtained for oxygen and fluorine doping in Hg-1201, the analysis shows a different oxygen ordering exhibited by Hg-1212. Moreover, for all studied cases, the experimental results show that at a local scale there is non uniform oxygen distribution. A series of *ab initio* EFG calculations allowed to infer that at low concentrations, regions without oxygen coexist with regions where $\text{O}_{2\delta}$ dumbbell molecules are located at the center of the Hg mesh. On the other side, at high concentrations, $\text{O}_{2\delta}$ dumbbell molecules coexist with single O_δ atoms occupying the center of the Hg mesh. The present results suggest that oxygen sits on the Hg planes in the form of a molecule and not as a single atom.

DOI: [10.1103/PhysRevB.84.094524](https://doi.org/10.1103/PhysRevB.84.094524)

PACS number(s): 74.72.Gh, 71.15.Mb, 75.40.—s

I. INTRODUCTION

Nowadays it is well accepted that the presence of dopants in high T_c superconductor (HTSC) cuprates strongly affects the behavior of these compounds, causing structural and electronic inhomogeneities.^{1,2} The existence of intrinsic inhomogeneities inherent to doping has become a central question of the physics of HTSC cuprates. In particular, how these inhomogeneities affect the superconducting transitions and the relationship between charge ordering and doping are topics under review.^{3–6}

In contrast to conventional superconductors, cuprates are randomly doped systems leading to atomic-scale variations in their chemical and electronic structure. The most remarkable examples are the hole-doped cuprates, where superconductivity appears when the antiferromagnetic insulating parent is doped with holes.⁷ This mechanism is generally related to a distribution of different dopant ions inducing charge transfer to the CuO_2 layers. This distribution leads to a chemical and electronic local disorder, diverging from the average structure, which definitely interferes with the electronic mechanism of superconductivity in these materials.^{1,8} Local disorder has been observed experimentally using techniques such as scanning tunneling microscopy,^{1,9} angle-resolved photoinduced emission spectroscopy,¹⁰ nuclear magnetic resonance,^{11,12} synchrotron radiation micro-x-ray diffraction,² among others. Some of these experiments have revealed that the nanoscopic disorder is correlated with the location of interstitial oxygen dopant atoms,^{1,8} suggesting a strong interplay between the dopant atoms and the local electronic properties in these materials.

Among the cuprate superconductors, the mercury-based family $[\text{HgBa}_2\text{Ca}_{n-1}\text{Cu}_n\text{O}_{2n+2+\delta}]$, also denoted as Hg-12($n-1$) n is a good prototype to study the existence of disorder

or inhomogeneities on the atomic scale due to their simple tetragonal structure and record T_c 's (132 K for the third member of the series¹³). As with all cuprate superconductors, the Cu-O plane is the main structural and electronic unit. These planes are linked by O-Hg-O chains involving apical oxygen atoms in a stable dumbbell coordination.

Disorder at the Hg planes is reported and believed to be associated with mercury deficiency and/or to nonstoichiometric excess oxygen (O_δ).^{14,15} Moreover, the doping level at the CuO_2 planes was found to be considerably lower than expected from the extra O_δ content following formal ionic considerations.^{16,17} These discrepancies have been attributed to the presence of single charged oxygen anions^{16,18} or *nonoxidizing* oxygen atoms, although, to the best of our knowledge, there is no experimental evidence for this fact.¹⁹ Therefore, the role of O_δ in the formation of charge inhomogeneities and its impact on the local electronic and structural properties, is of great importance.

The purpose of this paper is to contribute to a better understanding of O_δ interaction with the host lattice on the nanoscopic scale by using a local probe nuclear technique. Previous atomic-scale studies of oxygen and fluorine dopants have been performed mainly in the first member of this series of compounds (Hg-1201).^{14,20,21} To achieve higher O_δ concentrations, we have chosen the second member of this series, Hg-1212. To study the site occupancy of O_δ in Hg planes, the perturbed angular correlation (PAC) technique was applied in a similar way as in Refs. 20 and 21, where Hg-1201 was studied as a function of oxygen (O_δ) and fluorine (F_δ) concentrations. This technique is very well suited to probe the Hg neighborhood by measuring the electric field gradients (EFGs) at $^{199\text{m}}\text{Hg}$ nuclei. To fully grasp the PAC experimental results, *ab initio* charge-density calculations

have been performed using the WIEN code,²² where relaxed superlattices for different concentrations and configurations of the dopant O_δ were simulated.

II. EXPERIMENTAL DETAILS

Polycrystalline Hg-1212 samples were synthesized at CNRS/Grenoble using the high pressure–high temperature technique (HP-HT). A stoichiometric mixture of HgO and $Ba_2CaCu_2O_{6+\delta}$ was placed in a gold capsule and then treated at 1.6 GPa, 1073 K for 1 h, using a Conac-type hydraulic press.²³ To control sample quality, x-ray diffraction (XRD) measurements have been performed using a Siemens D5000 diffractometer, in transmission mode, with Cu $K\alpha$ radiation ($\lambda = 1.541 \text{ \AA}$), in a 2θ range between 10° and 90° . The lattice parameters were refined using the LeBail method with the program FULLPROF Suite.²⁴ Magnetic characterization was performed using a Quantum Design superconducting quantum interference device (SQUID) magnetometer in the range 4–150 K under an applied field of 0.005 T in zero-field-cooled (ZFC) and field-cooled procedures (FC). Since these samples are highly hygroscopic, the samples have been kept in a dry atmosphere and enclosed in sealed containers. The same macroscopic characterizations have been applied after the PAC experiments to survey the sample's quality.

In order to study the oxygen ordering in the mercury planes, PAC experiments have been performed. Following a similar procedure as in Refs. 20 and 21, Hg-1212 samples were implanted at room temperature with ^{199m}Hg ($T_{1/2} = 42 \text{ min}$) to a low dose of $3.5 \times 10^{12} \text{ at. cm}^{-2}$ and 55 keV energy at the ISOLDE/CERN facility.²⁵ Each PAC sample consisted of $\sim 10 \text{ mg}$ of powder. The implantation and sample transfer between the glove box and the implantation chamber were done in rough vacuum. All manipulations were performed inside a glove box under dry atmosphere. After implantation, each sample was annealed at 463–473 K under different atmospheres: in gas flow (argon or oxygen) or under pressurized oxygen, up to 152 bars. After annealing the samples were sealed inside copper containers, under dry air at ambient pressure. All PAC measurements were done after these preliminary thermal treatments, using a highly efficient PAC γ -ray BaF_2 detector setup.²⁶ The measurements were performed at room temperature and 77 K, using a liquid-nitrogen cryostat, covering the superconducting transition of the original raw Hg-1212 material. Table I summarizes the experimental conditions used in this paper, presented together with the relevant parameters obtained with the PAC data analysis.

The relevant information taken from the PAC measurements is obtained from the time perturbation function $R(t)$, modulated by the interaction of the quadrupole moment of the 158-keV intermediate state in the ^{199m}Hg decay cascade

TABLE I. Preliminary annealing conditions and EFG fitting parameters of the experimental $R(t)$ PAC functions. The first column refers to the experiments presented in Figs. 2 and 3. The average values were calculated over the two temperatures.

Experiment	Preliminary annealing conditions	Measurement temperature (K)	E1					E2					E3				
			f_1 (%)	ν_{Q1} (MHz)	$ V_{zz} _1$ ($V/\text{\AA}^2$)	η_1	δ_1	f_2 (%)	ν_{Q2} (MHz)	$ V_{zz} _2$ ($V/\text{\AA}^2$)	η_2	δ_2	f_3 (%)	ν_{Q3} (MHz)	$ V_{zz} _3$ ($V/\text{\AA}^2$)	η_3	δ_3
2(a)	Argon	RT	31 ± 12	1392 ± 70	854 ± 98	0.01 ± 1	0.02 ± 4	69 ± 10	1267 ± 63	777 ± 89	0.20 ± 5	0.03 ± 3	—	—	—	—	—
3(a)	flow	77	38 ± 15	1392 ± 70	854 ± 98	0.01 ± 1	0.02 ± 4	62 ± 12	1164 ± 55	757 ± 88	0.31 ± 8	0.09 ± 1	—	—	—	—	—
2(b)	O ₂ flow	RT	42 ± 11	1441 ± 72	884 ± 102	0.09 —	0.01 ± 3	58 ± 7	1288 ± 64	791 ± 91	0.23 ± 3	0.02 ± 1	—	—	—	—	—
2(c)	8 bar Pressurized O ₂	RT	37 ± 6	1476 ± 74	906 ± 104	0 —	0.02 ± 1	63 ± 6	1209 ± 60	742 ± 85	0.20 ± 1	0.06 ± 2	—	—	—	—	—
2(d)	25 bar	RT	46 ± 9	1444 ± 72	886 ± 102	0.09 ± 1	0.05 ± 3	54 ± 10	1141 ± 57	700 ± 80	0.27 ± 2	0.04 ± 4	—	—	—	—	—
3(b)	Pressurized O ₂	77	24 ± 9	1474 ± 74	892 ± 102	0.01 ± 1	0.13 ± 3	76 ± 11	1178 ± 58	723 ± 83	0.20 ± 1	0.02 ± 1	—	—	—	—	—
2(e)	40 bar	RT	—	—	—	—	—	69 ± 10	1212 ± 60	744 ± 85	0.21 ± 4	0.10 ± 7	31 ± 8	788 ± 40	484 ± 56	0.86 ± 3	0.03 ± 1
3(c)	Pressurized O ₂	77	—	—	—	—	—	83 ± 10	1262 ± 62	774 ± 90	0.28 ± 1	0.12 ± 3	17 ± 9	828 ± 42	508 ± 58	0.74 ± 9	0.06 ± 1
2(f)	152 bar	RT	—	—	—	—	—	69 ± 10	1213 ± 60	744 ± 86	0.26 ± 1	0.07 ± 10	31 ± 8	854 ± 43	524 ± 60	0.76 ± 2	0.07 ± 3
3(d)	Pressurized O ₂	77	—	—	—	—	—	67 ± 8	1151 ± 56	706 ± 81	0.16 ± 4	0.15 ± 3	33 ± 9	818 ± 41	502 ± 58	0.98 ± 9	0.01 ± 1
Average values per EFG	—	—	—	1440 ± 72	883 ± 102	0.04 ± 5	0.035 ± 3	—	1215 ± 60	750 ± 86	0.23 ± 4	0.067 ± 3	—	822 ± 14	504 ± 9	0.84 ± 4	0.05 ± 1

with the EFGs generated by the charge distribution in the Hg surroundings.²¹

Thirty γ_1 (374 keV)- γ_2 (158 keV) coincidence time spectra $N_j(\theta, t)$ are recorded. Each spectrum is related to each detector pair with relative angles $\theta = 180^\circ$ ($j = 6$) and $\theta = 90^\circ$ ($j = 24$). The $R(t)$ experimental anisotropy ratio aims the evidence of the perturbation function by eliminating the exponential half-life component and the correction for different geometrical efficiencies, as described in Eq. (1):

$$R(t) = 2 \frac{\sqrt{\prod_j^6 N_j(180^\circ, t)} - \sqrt{\prod_i^{24} N_i(90^\circ, t)}}{\sqrt{\prod_j^6 N_j(180^\circ, t)} + 2 \sqrt{\prod_i^{24} N_i(90^\circ, t)}}, \quad (1)$$

where N_j/N_i are γ - γ coincidences spectra measured at $180^\circ/90^\circ$, after subtraction of the chance coincidence background.

The fits to the $R(t)$ experimental PAC functions were then calculated numerically by taking into account the full Hamiltonian for the nuclear quadrupole interaction.²⁷ The Hamiltonian for static quadrupole interactions, represented in the principal axis referential where the EFG tensor V_{ij} is diagonal and choosing $|V_{zz}| \geq |V_{yy}| \geq |V_{xx}|$, is given by

$$\mathcal{H} = \frac{\hbar \nu_Q}{4I(2I-1)} \left[3I^2 - I(I+1) + \frac{1}{2} \eta (I_+^2 + I_-^2) \right], \quad (2)$$

where $\nu_Q = eQV_{zz}/\hbar$ is the fundamental interaction frequency, $I = 5/2$ is the nuclear spin of the intermediate state of the ^{199m}Hg decay cascade where the PAC measurement is performed, and $\eta = (V_{xx} - V_{yy})/V_{zz}$ is the EFG axial asymmetry parameter.

The experimental perturbation function $R(t)$, for polycrystalline samples, may be described by the fit function as $R(t) = \sum A_{kk} G_{kk}$, where A_{kk} are the angular correlation coefficients and G_{kk} are the perturbation factors. G_{kk} contains all the information about the fields interacting with the nuclear quadrupole (and magnetic) moments of the probe atoms and can be described by

$$G_{kk}(t) = \sum_i f_i \sum_n^3 S_{kn}^i \cos(\omega_n^i t) e^{-\omega_n^i \delta t}. \quad (3)$$

During the fitting procedure, the frequencies ω_n ($\omega_0 = 0$) and corresponding amplitudes S_{kn} are obtained after the \mathcal{H} diagonalization for each fraction (f_i) of probes interacting with different EFG distributions. For the ^{199m}Hg case, with $I = 5/2$, three frequencies are observed per EFG, which are a function of ω_n and η . The exponential term accounts for the attenuation observed on the $R(t)$ spectra, representing the effect of a Lorentzian distribution of EFGs. Depending on its width and shape, the $R(t)$ attenuation reveals inhomogeneities on charge density mostly attributed to midrange and incoherently distributed point defects, e.g., Hg vacancies.

The PAC experimental results were interpreted with the help of *ab initio* charge-density calculations in relaxed superlattices for different configurations and concentrations of oxygen. These calculations have been performed using the WIEN2K (Ref. 22) code via the full potential augmented plane-wave method (FLAPW) approach. A detailed description of the calculations will be presented afterward in the text.

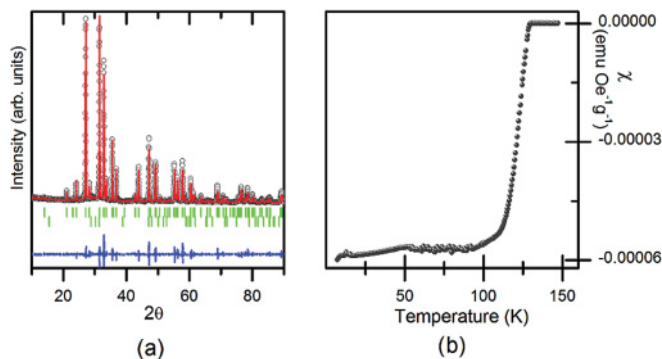


FIG. 1. (Color online) (a) XRD pattern obtained for the as-synthesized samples. (b) Temperature dependence of magnetic susceptibility.

III. RESULTS

A. Experiment

Figure 1 shows XRD and magnetic susceptibility results obtained from the as-synthesized samples in order to survey the samples quality. The Hg-1212 samples crystallize in the tetragonal structure, space group P_4mmm , with cell parameters $a = 3.869(8)$ Å and $c = 12.6746(6)$ Å, from where an extra oxygen content of 0.22(3) was inferred, in good agreement with the values reported in the literature.^{28,29} The samples are almost single phase with traces of CaHgO_2 . Magnetic measurements show a sharp transition with an onset critical temperature of ~ 128 K, in agreement with the previously reported values.^{28,29}

1. Room temperature PAC experiments

Figure 2 displays representative experimental perturbation functions $R(t)$ (left-hand side) and corresponding Fourier transforms (right-hand side) for samples annealed under different conditions. In a first step all measurements have been performed at room temperature. The high-quality fits are shown by continuous lines in the $R(t)$ spectra. The resulting fitting parameters are summarized in Table I. The fitting procedure used in this analysis took into account three EFG distributions per fit. A EFG_D distribution was included to account for the attenuation observed in all spectra and thus to improve the quality of the fits. This EFG_D is believed to be due to probes out of regular sites (nonannealed sites) in the Hg-1212 lattice and/or in the secondary phase CaHgO_2 present in the samples. A constant fraction of $\sim 20\%$ of the probes was assumed to be interacting with EFG_D , which is characterized by $\nu_Q \sim 585(80)$ MHz and $\delta \sim 0.43(3)$. The asymmetry parameter was set to zero since the attenuation is too high and does not allow to be determined. Since EFG_D is not representative of ^{199m}Hg in regular sites of the Hg-1212 phase, it will be excluded from the discussion. We stress that in the following when E1, E2, E3 are referred to and/or discussed, the sum of their relative fractions has been normalized to 100%.

Globally, the differences found in the experimental $R(t)$ functions, as measured in the Hg-1212 phase, can be attributed to the different annealing conditions, under argon or oxygen gas flow, or under pressurized oxygen. When performing the

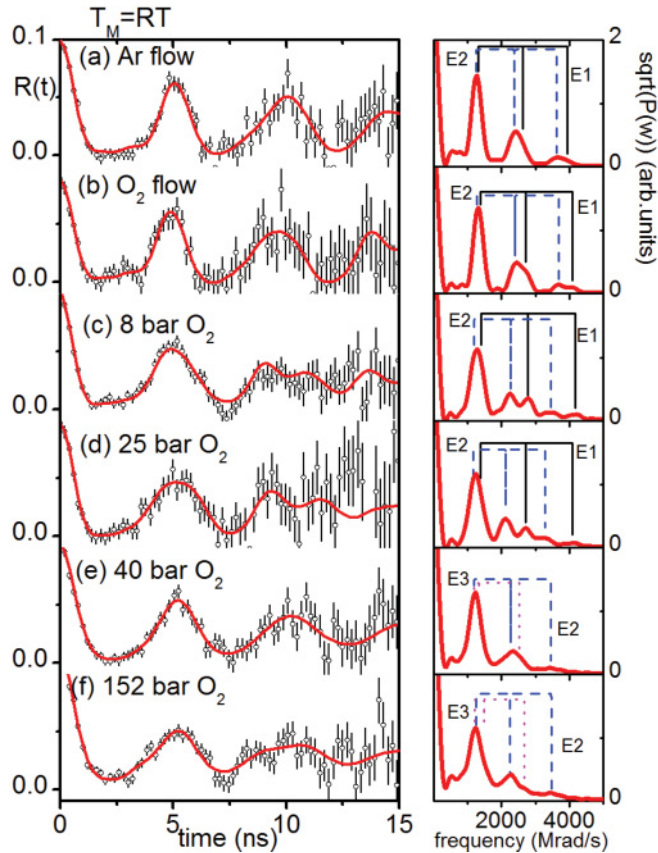


FIG. 2. (Color online) (a)–(f) (Left-hand side) Experimental perturbation functions $R(t)$ and (right-hand side) corresponding Fourier transforms. The thicker lines over the spectra are the fitting functions. Each EFG (abbreviated by E1, E2, and E3) is represented by its respective frequency triplet, plotted as vertical lines.

annealing step at 473 K under argon flow, the spectrum of Fig. 2(a) displays two electric field gradient distributions, named E1 and E2. The dominant distribution E2 characterizes 69(10)% of the ^{199m}Hg probes and is described by $\nu_{Q2} = 1267(63)$ MHz and an asymmetry parameter $\eta_2 = 0.21(1)$. Due to the fact that the Hg planes are similar for all members of this superconductor family and the EFG has a highly local sensitivity, one can refer to Ref. 20 to assign this nonaxially symmetric distribution as corresponding to ^{199m}Hg nuclei placed in lattice sites with symmetry lower than tetragonal as a consequence of the existence of a single O_δ in the center of the Hg mesh. An axial symmetric distribution is also observed for 31(12)% of the probe atoms interacting with it. This EFG, named E1, is described by $\nu_{Q1} = 1392(70)$ MHz and a nil asymmetry parameter. This distribution is also consistent with the results reported in Refs. 20 and 21 corresponding to ^{199m}Hg nuclei placed on regular sites of the Hg-1212 lattice without O_δ or other point defects in their nearest neighborhood.

Figure 2(b) shows the result of an experiment that was performed after annealing in oxygen flow. Once again, a main EFG distribution [58(7)% of the ^{199m}Hg probes] was found to be interacting with a nonaxially symmetric EFG (E2), as found in the argon flow annealing case. Most likely, this result shows that the doping during the synthesis prevails over the present annealing procedure. A fraction of 42(11)% of the probes was

found to be free of O_δ , as revealed by the axially symmetric EFG (E1).

Figures 2(c)–2(f) present the results obtained after annealing in pressurized oxygen. The data show essentially two distinct results depending on the applied pressures. For lower pressures, up to 25 bars, the same frequency triplets are found as in the previous experiments under argon and oxygen flow. The results only show slight changes in the fractions of ^{199m}Hg probe nuclei interacting with E1 and E2: 54–63% of Hg atoms interact with a single O_δ that originates at E2 and 37–46% of Hg atoms still do not have any O_δ in their neighborhood (E1). When higher pressures were applied, strong changes were observed, as shown in Figs. 2(e) and 2(f). E2 is still the dominant EFG as in previous cases, assigned to 69(10)% of the Hg atoms interacting with a distribution characterized by $\nu_{Q2} \sim 1212(60)$ MHz and $\eta_2 \sim 0.25(4)$. However, a unique and highly asymmetric EFG (named E3) is observed, being characterized by $\nu_{Q3} \sim 800(40)$ MHz and $\eta_4 = 0.8\text{--}0.9$, which affects 31(8)% of the Hg atoms. E3 is not explained by any of the calculated configurations reported so far in the literature^{20,21} and hints at the existence of a different oxygen configuration in the Hg planes that requires different O_δ configurations that are yet to be simulated.

2. 77-K PAC measurements

To further study possible changes of the O_δ configurations at low temperature, below the T_c of the raw samples, measurements in liquid nitrogen have been performed. Representative experimental $R(t)$ spectra (left-hand) and their respective Fourier analysis (right-hand) are displayed in Fig. 3, being the resulting fitting parameters also summarized in Table I.

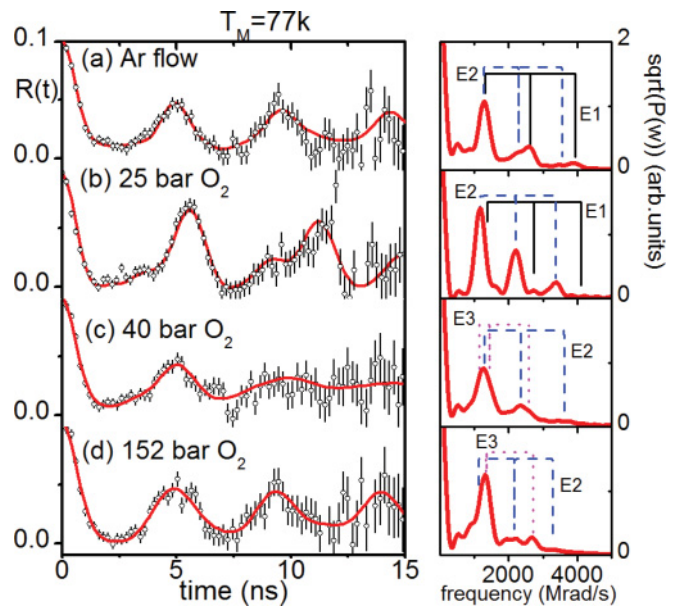


FIG. 3. (Color online) (a)–(d) (Left-hand side) Experimental perturbation functions $R(t)$ and (right-hand side) corresponding Fourier transforms. The thicker lines over the spectra are the fit functions. Each EFG (abbreviated by E) is represented by its representative frequency triplet, plotted as vertical lines.

Essentially, the experimental results show the same type of EFG distributions as found in the room-temperature measurements. Also here the same fitting procedure has been applied.

Figure 3(a) shows the experimental PAC results as measured at 77 K for a sample annealed in argon flow, revealing the same frequency triplets as found in the room-temperature measurement. The main EFG [E2, $f_2 = 62(8)\%$] is described by $\nu_{Q2} = 1164(55)$ MHz and an axial asymmetry parameter $\eta_2 = 0.31(6)$, which is slightly higher than the one characterizing this EFG at room temperature. An axially symmetric EFG (E1) was also found for 38(10)% of the probe Hg atoms and is characterized by $\nu_{Q1} = 1392(70)$ MHz and $\eta = 0.01(1)$.

Figure 3(b) shows $R(t)$ data for the sample annealed at 25 bars where one can observe two EFGs. The dominant EFG (E2) corresponds to 76(11)% of the probes interacting with a nonaxial symmetric distribution characterized by $\nu_{Q2} = 1178(58)$ MHz and $\eta_2 = 0.20(1)$. Approximately 24% of the probe ^{199m}Hg nuclei are free of O_δ , as revealed by the axially symmetric EFG (E1) characterized by $\nu_{Q1} = 1454(74)$ MHz and $\eta_1 = 0$.

When higher pressures were applied [Figs. 3(c) and 3(d)], the unique and highly asymmetric EFG (E3) appears as observed in the room-temperature measurements. E3 now affects 17–33% of the probes, depending on the annealing oxygen pressure. At 77 K, E3 parameters are not much different from the room-temperature measurements with $\nu_{Q3} \sim 820(41)$ MHz and a high asymmetry parameter that is almost one in the specific case of the sample annealed at 152 bars. In these measurements the dominant EFG (E2) is described by $\nu_{Q2} = 1151\text{--}1262$ MHz, $\eta \sim 0.16\text{--}0.28$ that affects $\sim 67\text{--}83\%$ of the probes.

The PAC measurements performed at room temperature and 77 K show equivalent results, mainly depending from the previous annealing treatment. Due to this similarity, average EFG parameters for E1, E2, and E3 were calculated and are summarized also in Table I.

Based only on the experimental data and previous literature results, some conclusions can be already drafted. The compound presents nonuniform oxygen distribution in which different oxygen-doped regions are found to coexist. In more detail, the annealing in argon flow was not sufficient to reduce the initial, as-synthesized O_δ content. The PAC results revealed a dominant EFG distribution E2, which hints at a diluted concentration of interstitial O_δ in the Hg planes. The annealings in oxygen flow and at oxygen pressures up to 25 bars did not change the system. When higher oxygen pressures were applied, 40 and 152 bars, there is no more evidence of Hg atoms free of O_δ in their neighborhood (no evidence for E1) and a highly asymmetric EFG appears, which hints to a unique O_δ configuration at higher concentrations.

To interpret these experimental results, simulations of different supercells with different oxygen concentrations and configurations were performed. These calculations are described in the following section.

B. EFG simulations

To fully grasp the PAC experimental results and extract the maximum information, EFG *ab initio* calculations have been

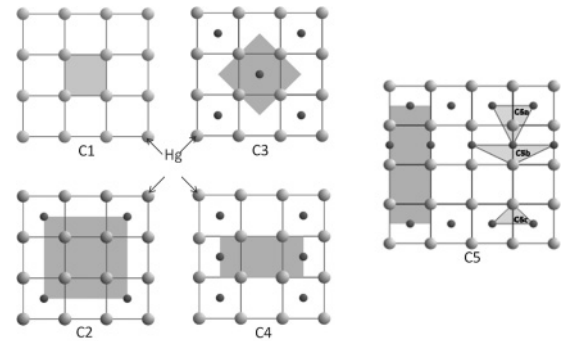


FIG. 4. Representation of the Hg planes of Hg-1212 as viewed along the c axis. Shaded regions represent supercells with different O_δ concentrations ($\delta = 0\text{--}0.66$).

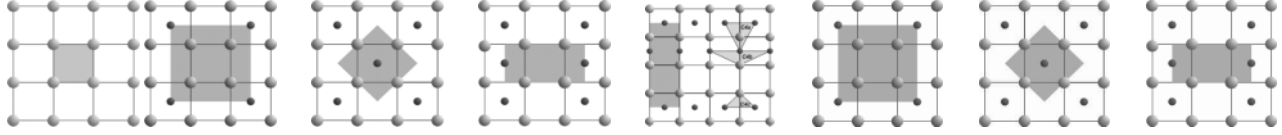
performed using the code WIEN2K (Ref. 22) via the FLAPW method with the generalized gradient approximation³⁰ (GGA) for the density functional. The FLAPW method is considered to be one of the most reliable methods in the calculation of EFG parameters, only requiring crystalline structure parameters (lattice constants and atomic positions) as input information, which in this paper were taken from neutron-diffraction experiments^{31,32} accounting for different oxygen dopings. To illustrate different O_δ doping configurations, various supercells have been constructed assuming the composition $\text{Hg}_m\text{Ba}_{2m}\text{Ca}_m\text{Cu}_{2m}\text{O}_{6m+n}$. Following earlier works,^{20,21} the simulations here implemented describe different configurations of single O_δ atoms all sitting within the Hg planes, including also particular ones where the dopant is represented by a dumbbell $\text{O}_{2\delta}$ molecule (with a 1.3-Å bond length as stabilized after relaxation), with the symmetry axis parallel to the c axis at the center of the Hg mesh. Only O_δ or $\text{O}_{2\delta}$ configurations which provide relevant information for the explanation and discussion of the experimental data are reported here. One should stress that the aim of the different supercells is to provide understanding of which local configurations of O_δ or $\text{O}_{2\delta}$ can originate the measured EFGs at the Hg site. It has been shown in previous works^{20,21} that the first-neighbor contribution dominates the EFG, allowing to infer the organization of O_δ atoms and/or dumbbells in the neighborhood of the ^{199m}Hg probing nuclei. With these considerations in mind, one shall further note that in each different supercell volume a nominal oxygen dopant local concentration can be assigned.

Figure 4 illustrates a schematic view of the built supercells projected along the c axis onto the Hg planes. The shaded regions represent the ab plane of the supercells used in the simulations. Since similar configurations were used for both O_δ and $\text{O}_{2\delta}$ cases, only one set of pictures is represented. The resulting EFG parameters found for Hg and for all other atoms in each supercell are summarized in Table II.

Figure 4(C1) shows the undoped supercell with $m = 1$ and $n = 0$, where there is no dopant oxygen in the neighborhood of Hg atoms. This supercell has the highest $|V_{zz}|_{C1}$ at the Hg site and nil asymmetry parameter due to the tetragonal symmetry.

In order to calculate the effect of the single O_δ doping in the Hg planes, four doped supercells have been constructed with nominal δ of 0.25, 0.50, and 0.66. Figure 4(C2) shows

TABLE II. Calculated EFG parameters for the Hg atoms on the relaxed Hg-1212 + single O_δ /dumbbell $O_{2\delta}$ supercells. The inserted figures show the Hg planes of the different supercells, presented as shadowed regions. Light/dark symbols represent Hg/O atoms.



Supercell	Supercell C1		Supercell C2		Supercell C3		Supercell C4		Supercell C5		Supercell C2*		Supercell C3*		Supercell C4*	
	$\delta O = 0$		$\delta O = 0.25$		$\delta O = 0.50$		$\delta O = 0.50$		$\delta O = 0.66$		$\delta O = 0.25$		$\delta O = 0.50$		$\delta O = 0.50$	
	V_{zz}	η														
	(V/Å ²)		(V/Å ²)		(V/Å ²)		(V/Å ²)		(V/Å ²)		(V/Å ²)		(V/Å ²)		(V/Å ²)	
Hg_a	-734.96	0	-561.81	0.734	-572.39	0.661	-496.39	0.023	-598.78	0.080	-694.40	0.156	-661.98	0.327	-669.48	0.049
Hg_b	—	—	—	—	—	—	—	—	-547.74	0.703	—	—	—	—	—	—
Hg_c	—	—	—	—	—	—	—	—	86.23	0.091	—	—	—	—	—	—

the supercell ($m = 4$, $n = 1$) where Hg atoms interact with one single dopant oxygen, which is located in the center of the Hg mesh. C2 shows a nonsymmetric EFG with a lower $|V_{zz}|_{C2} \sim 562 \text{ V}/\text{Å}^2$ and a highly distorted local environment given by $\eta_{C2} = 0.7$.

Figures 4(C3) and 4(C4) display two local configurations ($m = 2$ and $n = 1$ supercells) existing for Hg atoms interacting with two O_δ , both having the same nominal concentration $\delta = 0.50$. Even if these two configurations have the same nominal δ , the different oxygen rearrangement causes changes in the EFG parameters. The supercell C3 represents O_δ arranged in a checkerboardlike pattern where the Hg- O_δ bonds make a 180° angle. In this case, $|V_{zz}|_{C3} = 572 \text{ V}/\text{Å}^2 \sim |V_{zz}|_{C2}$ and $\eta_{C3} = 0.66$ is slightly lower than η_{C2} . The simulation represented by the supercell C4 corresponds to the situation where O_δ is distributed along interstitial rows parallel to the b axis and the Hg- O_δ bonds make a 90° angle. C4 has a lower $|V_{zz}|_{C4} = 496 \text{ V}/\text{Å}^2$ than the previous cases and an almost nil asymmetry parameter $\eta_{C4} \sim 0.02$.

Figure 4(C5) ($m = 3$, $n = 3$) shows a supercell with three nonequivalent Hg atoms leading to different EFG parameters. C5 was created to understand if, under O_δ high concentrations, interstitial Hg-Hg bonds could be occupied. This supercell shows quite diverse $|V_{zz}|$ and η values depending on the nonequivalent Hg atoms. The atom noted as C5a has $|V_{zz}|_{C5a} = 598 \text{ V}/\text{Å}^2$, comparable to the values presented by C2 and C3 configurations; however, the axial asymmetry parameter $\eta_{C5a} = 0.08$ is almost nil. The Hg atom, denoted as C5b, has a highly asymmetric local environment with $\eta_{C5b} = 0.7$, though its $|V_{zz}|_{C5b} = 548 \text{ V}/\text{Å}^2$ is also in the same range of C2, C3, and C5a. The third nonequivalent Hg atom (C5c) has the smallest $|V_{zz}|_{C5c} = 86 \text{ V}/\text{Å}^2$ and an axially symmetric local environment revealed by $\eta_{C5c} \sim 0.09$. It is further pointed that interstitial O_δ along Hg-Hg bonds alone is not stable. Therefore, the C5 supercell was designed as the simplest distribution of O_δ that could stabilize the oxygen dopant in the Hg-Hg bonds.

The configurations C2, C3, and C4, now denoted by C2*, C3*, and C4*, have been further used assuming the location of a $O_{2\delta}$ dumbbell molecule instead of a single O_δ in the Hg planes.

As expected, the insertion of a molecule in the Hg planes led to changes in the EFGs at the Hg site regarding single O_δ cases. The C2* supercell shows a configuration where Hg atoms interact with one $O_{2\delta}$ dumbbell, with local nominal $\delta = 0.5$, which is located at the center of the Hg mesh. Differently from C2, this configuration originates a slightly nonaxially symmetric EFG with $|V_{zz}|_{C2}^* = 694 \text{ V}/\text{Å}^2$ and $\eta_{C2}^* = 0.16$. The two local configurations C3* and C4* have now nominal local $\delta = 1$. C3* reproduces the checkerboardlike pattern, although the resulting EFG parameters are different from C3 with $|V_{zz}|_{C3}^* = 662 \text{ V}/\text{Å}^2$ and $\eta_{C3}^* = 0.33$. In the C4* configuration, the Hg atoms interact with oxygen dumbbells distributed along rows parallel to the c axis. In this case, an axially symmetric EFG with $|V_{zz}|_{C4}^* = 670 \text{ V}/\text{Å}^2$ and $\eta_{C4}^* = 0.05$ is found.

Some conclusions can be already drafted based on the calculated data, which will serve later for the analysis of the experimental data. The calculations have been performed for different $O_\delta/O_{2\delta}$ doping configurations, considering both unrelaxed and relaxed supercells. The relaxation of the atomic positions is done in a self-consistent way by minimizing atomic forces, which has important effects on some of the atomic internal parameters.

Figure 5 shows a three-dimensional (3D) artistic view of the relaxed C2, C3, and C4 supercells to help visualize these atomic shifts. The atomic relaxation resulting from the C2*, C3*, and C4* supercells are not presented since they are smaller than the single O_δ cases. The structural relaxation has a major effect on the barium and apical oxygen sites [O(2)], where strong shifts in the c axis are observed due to the placement of O_δ in the interstitial sites of the Hg mesh. This effect can be explained in the frame of an ionic picture where positive Ba ions are more attracted to the Hg-doped layer while the apical oxygen atoms are further repelled. Consequently, the EFG at the Hg site was found to be largely affected from one configuration to the other, depending essentially on the symmetry and local relaxations.

The simulations with the oxygen dumbbell molecule show less asymmetric local environments than the ones obtained with single O_δ atoms. On the other hand, the $|V_{zz}|$ magnitude shows an increase when compared with the single O_δ values,

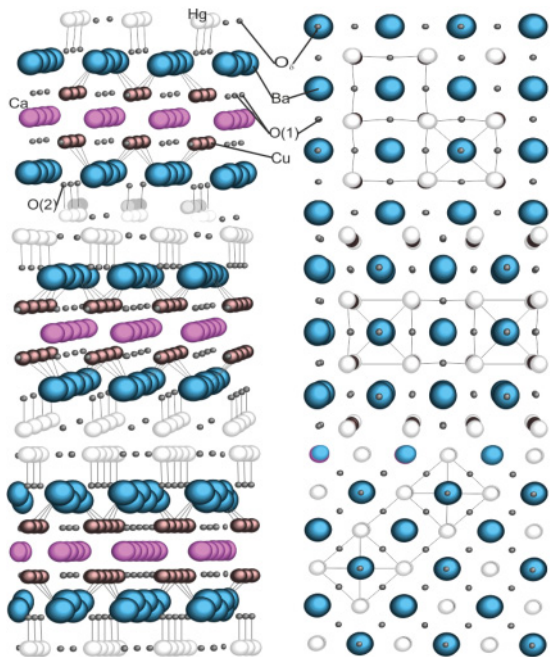


FIG. 5. (Color online) Artistic view of the Hg-1212 supercell structures C2, C3, and C4, as obtained from the FLAPW calculations, which were used to calculate the EFGs: (Left-hand side) projections of the lattice along the c axis and (right-hand side) projections along the plane perpendicular to the c axis.

though all $|V_{zz}|$ are quite similar, ranging between 670 and 700 $\text{V}/\text{\AA}^2$. Following again an ionic picture, the existence of a molecule sharing less charge than a single O_δ causes smaller shifts in the barium and apical oxygen positions, leading to smaller variations on $|V_{zz}|$ and η .

Figure 6 plots relative z coordinates for barium and apical oxygen along the c axis as calculated for the C configurations, together with available data taken from literature, as a function of δ . When nonequivalent atomic positions exist for barium, the points represent the average calculation accounting for the multiplicity of the nonequivalent atoms. For completeness

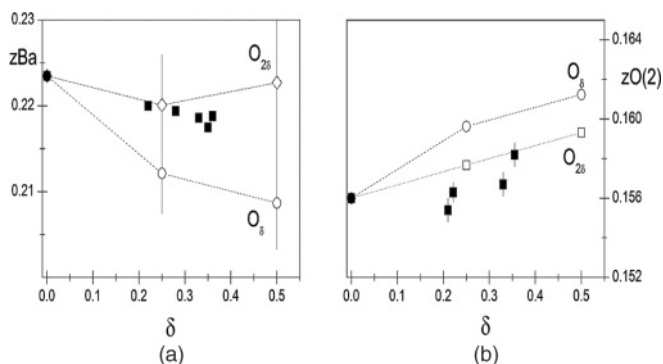


FIG. 6. Plot of relative z coordinates for barium and apical oxygen as a function of dopant oxygen δ , reported in the literature (Refs. 28,29,33 and 34) (black symbols), from FLAPW calculations for different supercells with single O_δ (open circles) and with $\text{O}_{2\delta}$ dumbbell molecules (open squares). The calculated values are normalized to the neutron powder diffraction (NPD) experimental ones for the undoped case.

of discussion, the parameters of the C^* configuration are included, keeping in mind that the true local dopant oxygen concentration of this supercell is obtained by multiplying δ by two, due to the dumbbell configuration.

IV. DISCUSSION

When comparing the average experimental EFG parameters ($|V_{zz}|$ and η) with the simulated ones at the Hg sites (summarized in Table II), it is possible to observe a good matching for some cases of the simulated configurations.

Figure 7 plots the experimental and simulated EFG values for clearness of discussion. The axially symmetric experimental distribution E1 is assigned to Hg atoms in regular sites of the lattice without dopant oxygen or other defects in their neighborhood, corresponding to the EFG calculated within the C1 configuration. This EFG has the highest $|V_{zz}|$ and a nil asymmetry parameter, in agreement with previous reports on Hg-1201.^{20,21} Still, $|V_{zz}|_{\text{C1}}$ is smaller than the one observed experimentally, though the nil asymmetry parameter allows the correct assignment to the C1 configuration.

The nonaxially symmetric EFG distribution E2 is best assigned to C2^* , where both experimental and simulated EFG parameters are in good agreement. The supercell C3^* gave similar $|V_{zz}|$ parameters to C2^* , but the experimental asymmetry parameter η favors the C2^* configuration. This result evidences that the $\text{O}_{2\delta}$ molecules might be competing with single O_δ atoms when doping these compounds. We point out that only single O_δ atoms were reported for Hg-1201,²¹ but in that work the determinant factor for the EFG parameter calculation, i.e., structural relaxation, could not be taken into account in the simulations. Additionally, the existence of $\text{O}_{2\delta}$ molecules was not considered there. In the present C2^* configuration each Hg atom interacts with a oxygen dumbbell molecule which is located in interstitial sites in the center of the Hg mesh with relative coordinates $(\pm 1/2, \pm 1/2, z_{\text{Hg}})$.

The highly asymmetric experimental distribution E3 presents EFG parameters which, in a direct comparison with the calculated data, could be assigned to more than one configuration. C4 and C4^* configurations of O_δ or $\text{O}_{2\delta}$ that would correspond to stripelike ordering of the dopants do not find an experimental equivalent. The good matching between the experimental and simulated $|V_{zz}|$ and η is found for C2, C3, and C5 configurations, where only single O_δ atoms play a role. Starting with the C5 supercell, at first glance, one of the three nonequivalent Hg atoms (C5b) could explain the experimental distribution E3. However, the present simulations have shown that the C5b configuration is not stable alone, without O_δ in adjacent cells. Therefore, the other two EFGs generated by C5a and C5c should be experimentally observed. However, the fitting analysis has excluded these two EFGs; consequently, the full C5 configuration is excluded, which agrees with the assumption that dopant O_δ atoms cannot occupy interstitial Hg-Hg bonds. In fact, the location of O_δ atoms in the Hg-Hg bonds was found to be energetically stable only in the cases of partial substitution of Hg by Cu.^{19,35}

Looking now to C2 and C3 configurations, the direct comparison between simulated and experimental EFG parameters is not sufficient to clearly assign one of these configurations. Therefore, an estimation of the dopant concentration δ_{PAC}

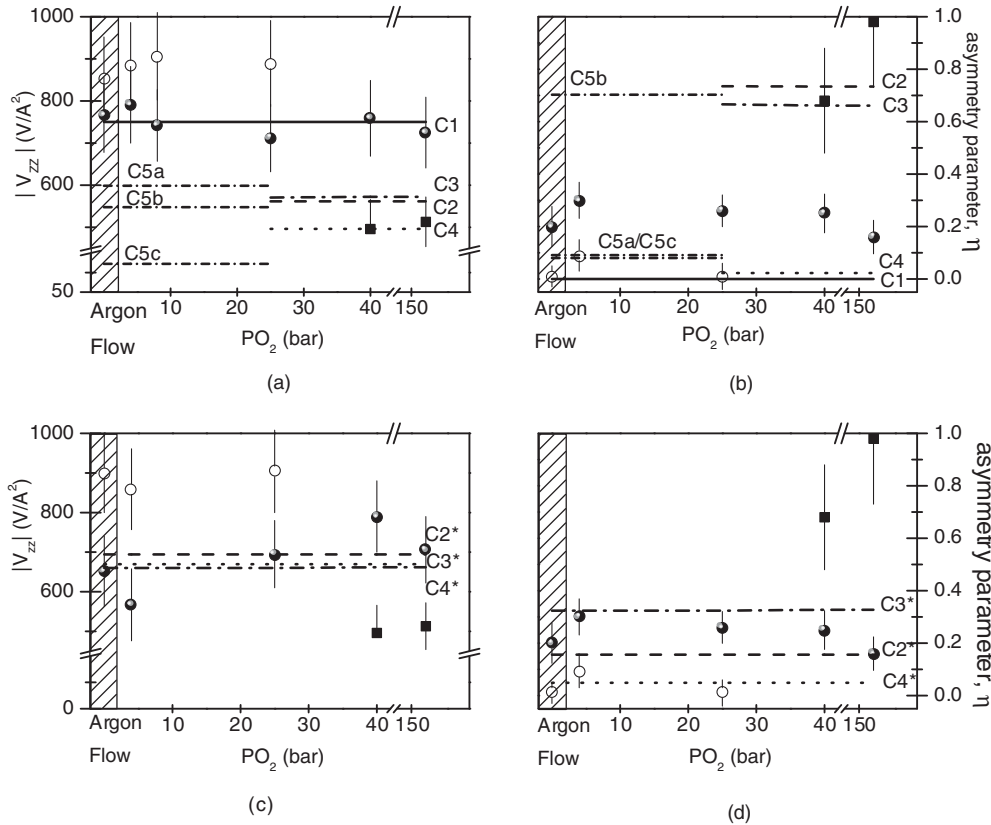


FIG. 7. Experimental and simulated EFG parameters (main component of the EFG tensor V_{zz} and the asymmetry parameter η) for Hg-1212+single O_δ and Hg-1212+dumbbells $O_{2\delta}$ [(c) and (d)] supercells. The horizontal lines represent the calculated V_{zz} and η .

within the ^{199m}Hg probing sample region will be performed. It is reported that T_c has a cupolalike dependence with doping (δ), where $\delta_{\text{opt}} \sim 0.22(4)$ (Refs. 28,29,33, and 34) and $\delta_{\text{max}} \sim 0.30(3)$.^{28,29,33,34} From XRD measurements, the present samples after synthesis have $\delta = 0.22(3)$, which is in good agreement with the optimal doping for this compound. After PAC experiments, the oxygen abundances can be quite different. To infer δ_{PAC} from the PAC E1, E2, and E3 fractions, the number of single O_δ or $O_{2\delta}$ dumbbells interacting with the probing nuclei is considered. The EFG calculations showed that E2 accounts for the Hg atoms that have a single $O_{2\delta}$ dumbbell (C2*) in their neighborhood. Since each molecule can be *seen* by four Hg atoms, the corresponding δ_{PAC} abundance is given by $\delta_{\text{PAC}}(\text{C2}^*) = f_2/2$. Two abundances can be calculated depending on the assignment of E3 to either C2 or C3 configurations. Assuming, on the one hand, that each Hg atom has only one O_δ in its neighborhood (C2), the corresponding PAC abundance shall be given by $\delta_{\text{PAC}}(\text{C2}) = f_3/4$. On the other hand, if each Hg atom is surrounded by two O_δ , in a checkerboard configuration (C3), the abundance will be given by $\delta_{\text{PAC}}(\text{C3}) = f_3/2$. The total δ_{PAC} per sample is thus given by the sum of all contributions, assuming either C2 or C3 configurations coexisting with C2*. Assuming the coexistence of both C2* and C3, with estimated $\delta_{\text{PAC}} \sim 0.5$, the local doping abundances are well above the reported dopant concentration limit allowed for this compound, i.e., $\delta \sim 0.35$. Contrarily, the coexistence of C2* and C2 configurations leads

to $\delta_{\text{PAC}} \sim 0.4$, which is more compatible with the reported dopant concentrations.

Local dopant concentrations, as estimated from the PAC fractions, must be interpreted within the limited number of the dopant configurations here reported. Moreover, the present results suggest the existence of $O_{2\delta}$ molecules coexisting with single O_δ atoms.

These experiments hint at a break of the $O_{2\delta}$ dumbbell upon an oxygen pressure increase. This further suggests that single O_δ and $O_{2\delta}$ have different solubilities. The dynamics of this process might be related to the atomic mobility, to the charge of the dopant, and to the number of available copper planes in this type of compound. Additionally, these should be short-range effects since the ordering cannot build up coherently too far without originating deformed superlattices which would be seen by diffraction techniques. In fact, in the numerous neutron-diffraction and x-ray scattering studies,^{18,28,32,36,37} there was no indication or suggestion for the existence of molecules at the Hg planes. In addition, the nonuniform dopant local distribution, as found in this paper, complicates the analysis via techniques that make use of coherence or average oxygen concentration.

The existence of $O_{2\delta}$ in competition with O_δ in the Hg planes might also present a justification for the systematic differences reported between the measured atomic dopant concentration and the number of holes created at the copper planes.^{16,17} These differences have been attributed to the

existence of monovalent oxygen,¹⁶ showing that the ionic model is inappropriate to describe the hole doping mechanism. Nevertheless, those results do not exclude the presence of $O_{2\delta}$ molecules at the Hg planes, whose existence has been suggested by the presence of monovalent superoxide molecules (O_2^-) in $La_2CuO_{4+\delta}$.³⁸ Note that in FLAPW there is no unique way to assign separate charge-density regions to each atom, i.e., to clearly define the spatial confinement of charge of an ion, it shall be stressed that the calculations clearly showed that the charge transferred by the $O_{2\delta}$ molecules to the copper planes is much smaller than the one transferred by single O_δ atoms. Techniques such as electron paramagnetic resonance (EPR), IR spectroscopy, and mass spectrometry could be sensitive to the existence of low-concentration oxygen anomalies, but its detection and characterization is quite difficult. On the other hand, the PAC technique combined with powerful simulation techniques of atomic modeling provide unique ways to characterize nanoscopic phenomena which could not be unveiled in other ways. These studies would be ideally continued on single crystals where the orientation could be used to compare with the oxygen configuration models.

V. CONCLUSIONS AND PERSPECTIVES

The EFGs at the Hg site in Hg-1212 have been measured via the PAC technique as a function of oxygen doping. The assignment of each observed EFG was performed using *ab initio* charge-density calculations for a variety of oxygen

configurations. For all studied cases, nonlocal uniform oxygen distributions were found. At low oxygen concentrations, the data analysis suggests the presence of oxygen dumbbells located at the Hg planes in the center of the Hg mesh, coexisting with regions free of oxygen. At high oxygen concentrations, the oxygen dumbbells coexist with single oxygen atoms occupying the center of the Hg mesh. The present results suggest that oxygen sits at the Hg planes on the form of a molecule and not as single atoms. The existence of $O_{2\delta}$ in competition with O_δ may provide additional understanding for the justification for the systematic differences reported between the measured atomic dopant concentration and the number of holes created at the copper planes.

Experiments on the third compound of this family, Hg1223, shall provide complementary information on the oxygen doping as well as on the local behavior of Hg and its electronic environment as a function of temperature.

ACKNOWLEDGMENTS

This work was supported by the Portuguese Foundation for Science and Technology, FCT, with the project CERN-FP-109272-2009, by the German BMBF funding resources, and by the ISOLDE collaboration with approved project IS360. T.M.M. acknowledges FCT Ph.D. Grant No. SFRH/BD/29445/2006. The authors gratefully thank V. S. Amaral, P. Bordet, and T. Hansen for fruitful discussions, and M. B. Barbosa, R. P. Vilhena, and M. Bacia for support during experiments.

*Present address: IFIMUP and IN—Institute of Nanosciences and Nanotechnologies, Rua do Campo Alegre 687, P-4169-007 Porto, Portugal; taniamel@mail.cern.ch

¹K. McElroy, J. Lee, J. A. Slezak, D.-H. Lee, H. Eisaki, S. Uchida, and J. C. Davis, *Science* **309**, 1048 (2005).

²M. Fratini, N. Poccia, A. Ricci, G. Campi, M. Burghammer, G. Aeppli, and A. Bianconi, *Nature (London)* **466**, 841 (2010).

³K. I. Kugel, A. L. Rakhmanov, A. O. Sboychakov, F. V. Kusmartev, N. Poccia, and A. Bianconi, *Supercond. Sci. Technol.* **22**, 014007 (2009).

⁴F. V. Kusmartev and M. Saarela, *J. Supercond. Novel Magn.* **22**, 155 (2009).

⁵S. Pathak, V. B. Shenoy, M. Randeria, and N. Trivedi, *Phys. Rev. Lett.* **102**, 027002 (2009).

⁶T. Honma and P. H. Hor, *Phys. Rev. B* **77**, 184520 (2008).

⁷J. E. Hirsch, *Phys. Lett. A* **134**, 451 (1989).

⁸A. N. Pasupathy, A. Pushp, K. K. Gomes, C. V. Parker, J. Wen, Z. Xu, G. Gu, S. Ono, Y. Ando, and A. Yazdani, *Science* **320**, 196 (2008).

⁹A. Yazdani, *J. Phys. Condens. Matter* **21**, 164214 (2009).

¹⁰A. Damascelli, D. Hussain, and Z. X. Shen, *Rev. Mod. Phys.* **75**, 473 (2003).

¹¹K. Ishida, K. Yoshida, T. Mito, Y. Tokunaga, Y. Kitaoka, K. Asayama, A. Nakayama, J. Shimoyama, and K. Kishio, *Phys. Rev. B* **58**, R5960 (1998).

¹²Y. Itoh, J. Machi, S. Adachi, A. Fukuoka, K. Tanabe, and H. Yasuoka, *J. Phys. Soc. Jpn.* **67**, 312 (1998).

¹³A. Schilling, M. Cantoni, J. D. Gui, and H. R. Ott, *Nature (London)* **363**, 56 (1993).

¹⁴D. Rybicki, J. Haase, M. Greven, G. Yu, Y. Li, Y. Cho, and X. Zhao, *J. Supercond. Novel Magn.* **22**, 179 (2009).

¹⁵C. Ambrosch-Draxl and E. Ya. Sherman, *Phys. Rev.* **74**, 024503 (2006).

¹⁶D. J. Singh and W. E. Pickett, *Phys. Rev. Lett.* **73**, 476 (1994).

¹⁷E. Pellegrin, J. Fink, C. T. Chen, Q. Xiong, Q. M. Lin, and C. W. Chu, *Phys. Rev. B* **53**, 2767 (1996).

¹⁸Q. Huang, J. W. Lynn, Q. Xiong, and C. W. Chu, *Phys. Rev. B* **52**, 462 (1995).

¹⁹V. L. Aksenov, A. M. Balagurov, V. V. Sikolenko, V. G. Simkin, V. A. Alyoshin, E. V. Antipov, A. A. Gippius, D. A. Mikhailova, S. N. Putilin, and F. Bouree, *Phys. Rev. B* **55**, 3966 (1997).

²⁰J. G. Correia, H. Haas, V. S. Amaral, A. M. L. Lopes, J. P. Araujo, S. Le Floch, P. Bordet, E. Rita, J. C. Soares, and W. Tröger (ISOLDE Collaboration), *Phys. Rev. B* **72**, 144523 (2005).

²¹J. G. Correia, J. P. Araujo, S. M. Loureiro, P. Toulemonde, S. Le Floch, P. Bordet, J. J. Capponi, R. Gatt, W. Tröger, B. Ctorcecka, T. Butz, H. Haas, J. C. Marques, and J. C. Soares (ISOLDE Collaboration), *Phys. Rev. B* **61**, 11769 (2000).

²²P. Blaha, K. Schwarz, G. K. H. Madsen, D. Kvasnicka, and J. Luitz, WIEN2K—an augmented plane wave + local orbitals program for calculating crystal properties [www.wien2k.at].

²³P. Odier, A. Sin, P. Toulemonde, A. Bailly, and S. Le Floch, *Supercond. Sci. Technol.* **13**, 1120 (2000).

²⁴J. Rodriguez-Carvajal, *Physica B* **192**, 55 (1993).

- ²⁵E. Kugler, D. Fiander, B. Johnson, H. Haas, A. Przewloka, H. L. Ravn, D. J. Simon, and K. Zimmer, *Nucl. Instrum. Methods Phys. Res. Sect. B* **70**, 41 (1992).
- ²⁶T. Butz, *Nucl. Instrum. Methods Phys. Res. Sect. A* **284**, 417 (1989).
- ²⁷N. P. Barradas, M. Rots, A. A. Melo, and J. C. Soares, *Phys. Rev. B* **47**, 8763 (1993).
- ²⁸O. Chmaissem, L. Wessels, and Z. Z. Sheng, *Physica C* **230**, 231 (1994).
- ²⁹A. Kareiva, J. Barkauskas, and S. Mathur, *J. Phys. Chem. Solids* **61**, 789 (2000).
- ³⁰J. P. Perdew, K. Burke, and M. Ernzerhof, *Phys. Rev. Lett.* **77**, 3865 (1996).
- ³¹B. A. Hunter, J. D. Jorgensen, J. L. Wagner, P. G. Radaelli, D. G. Hinks, H. Shaked, and R. L. Hitterman, *Physica C* **221**, 1 (1994).
- ³²P. G. Radaelli, J. L. Wagner, B. A. Hunter, M. A. Beno, G. S. Knapp, J. D. Jorgensen, and D. G. Hinks, *Physica C* **216**, 29 (1993).
- ³³A. Fukuoka, A. Tokiwa-Yamamoto, M. Itoh, R. Usami, S. Adachi, H. Yamauchi, and K. Tanabe, *Physica C* **265**, 13 (1996).
- ³⁴E. V. Antipov, J. J. Capponi, C. Chaillout, O. Chmaissem, S. M. Loureiro, M. Marezio, S. N. Putilin, A. Santoro, and J. L. Tholence, *Physica C* **218**, 348 (1993).
- ³⁵X. Zhang, W. H. Lu, and C. K. Ong, *J. Phys. Chem. Solids* **60**, 1675 (1999).
- ³⁶Q. Huang, J. W. Lynn, R. L. Meng, and C. W. Chu, *Physica C* **218**, 356 (1993).
- ³⁷J. L. Wagner, B. A. Hunter, D. G. Hinks, and J. D. Jorgensen, *Phys. Rev. B* **51**, 15407 (1995).
- ³⁸K. H. Lee and R. Hoffmann, *J. Phys. Chem. A* **110**, 609 (2006).